J Nanopart Res (2009) 11:1393–1403
DOI 10.1007/s11051-008-9527-4

RESEARCH PAPER

Morphology of single-wall carbon nanotube aggregates generated by electrospray of aqueous suspensions

Bon Ki Ku · Pramod Kulkarni

Received: 30 May 2008 / Accepted: 20 September 2008 / Published online: 14 October 2008
© Springer Science+Business Media B.V. 2008

Abstract Airborne single-wall carbon nanotubes (SWCNTs) have a high tendency to agglomerate due to strong interparticle attractive forces. The SWCNT agglomerates generally have complex morphologies with an intricate network of bundles of nanotubes and nanoropes, which limits their usefulness in many applications. It is thus desirable to produce SWCNT aerosol particles that have well-defined, unagglomerated fibrous morphologies. We present a method to generate unagglomerated, fibrous particles of SWCNT aerosols using capillary electrospray of aqueous suspensions. The effects of the operating parameters of capillary electrospray such as strength of buffer solution, capillary diameter, flow rate, and colloidal particle concentration on the size distributions of SWCNT aerosols were investigated. Results showed that electrospray from a suspension of higher nanotube concentration produced a bimodal distribution of SWCNT aerosols. Monodisperse SWCNT aerosols below 100 nm were mostly non-agglomerated single fibers, while polydisperse aerosols larger than 100 nm had two distinct morphologies: a ribbon shape and the long, straight fiber. Possible mechanisms are suggested to explain the formation of the different shapes, which could be used to produce SWCNT aerosols with different morphologies.

Keywords Single-wall carbon nanotubes (SWCNTs) · Electrosprays · Water suspensions · Straight fiber · Aerosols · Agglomeration

B. K. Ku (✉) · P. Kulkarni
Centers for Disease Control and Prevention (CDC), National Institute for Occupational Safety and Health (NIOSH), 4676 Columbia Parkway, MS-R3, Cincinnati, OH 45226, USA
e-mail: BKu@cdc.gov

P. Kulkarni
e-mail: PSKulkarni@cdc.gov

Introduction

The generation of nanoaerosols with well-defined morphology is necessary in many applications such as instrument calibration and evaluation (Ku and Maynard 2005, 2006), material synthesis (Nakaso et al. 2001, 2002), and toxicity studies designed to understand the health effects of aerosol particles (Oberdörster et al. 2005). Single-walled carbon nanotubes (SWCNTs) are a class of engineered nanomaterials exhibiting unique physical and chemical properties. As applications of these materials continue to grow, there is an increasing concern over their possible implications to human health and environment (Oberdörster et al. 2005; Shvedova et al. 2005; Lam et al. 2006; Stern and McNeil 2008).

Due to the fibrous nature of SWCNT particles, concerns have been raised over the similarity of SWCNT particles to asbestos fibers in the context of their health effects (Baron et al. 2001; Poland et al. 2008). Research has shown that SWCNTs are

cytotoxic and may lead to oxidative stress in vitro (Shvedova et al. 2003), as well as indicating pro-inflammatory and fibrogenic responses in rodent lungs (Lam et al. 2004; Warheit et al. 2004; Shvedova et al. 2005; Warheit 2006). However, these studies lacked the complete characterization of particle morphologies; as a result, the role of particle morphology on the toxicological response is largely unknown. Part of the difficulty in conducting such toxicological studies is the persistent lack of robust methods to generate SWCNT aerosols with well-defined morphology.

A recent study showed that SWCNT particles generated by the high pressure CO disproportionation (HiPCO^{TM}) process are difficult to aerosolize, in the nanometer size range, directly from the powder phase using a mechanical agitation (using a vortex shaker) because of their extremely low bulk density (Maynard et al. 2004). Also, airborne particles generated from this technique are aggregates that consist of intricate network of bundles of individual nanotubes often self-assembled into ropes (from about 2 nm to >50 nm in diameter) (Maynard et al. 2007; Ku et al. 2007). While such aerosolization techniques are valuable to produce aerosols for general toxicological studies, they are hardly useful for studies that are designed to investigate the effect of particle morphology. In other applications, such as instrument response evaluation, well-defined morphologies of SWCNT aerosol particles are necessary.

In this article, we used a capillary electrospray method (Fernandez de la Mora and Loscertales 1994; Kaufman 2000; Ku et al. 2004) to aerosolize the colloidal SWCNT suspension to obtain aerosol particles that are relatively less agglomerated, and have well-defined fibrous nature. The electrospray method is capable of producing relatively small and less agglomerated aerosols due to the uniformity of droplet size and the ability to fine tune the initial droplet size. The method also produces highly charged aerosol that effectively minimizes aggregation, resulting in SWCNT aerosol with single fiber morphology. Electrospray has been widely used to generate a variety of nanomaterials (Kim and Pui 2005; Ku 2007); however, no studies to date have reported the generation of SWCNT particles using electrospray method.

Experimental

The experimental setup is similar to the one used in an earlier study (Ku et al. 2004). An electrospray aerosol generator (Model 3480, TSI Inc.) was used, but capillary tubes and fittings were modified and purchased from Polymicro Technologies. Figure 1 shows the details of modified electrospray setup. Purified SWCNTs (CNI, Houston, TX) were used, which were produced by the HiPCO^{TM} technique (Scott et al. 2003), employing CO in a continuous-flow gas phase as the carbon feedstock and $Fe(CO)_5$ as the iron-containing catalyst precursor, and which were purified by acid treatment to remove the metal contaminates

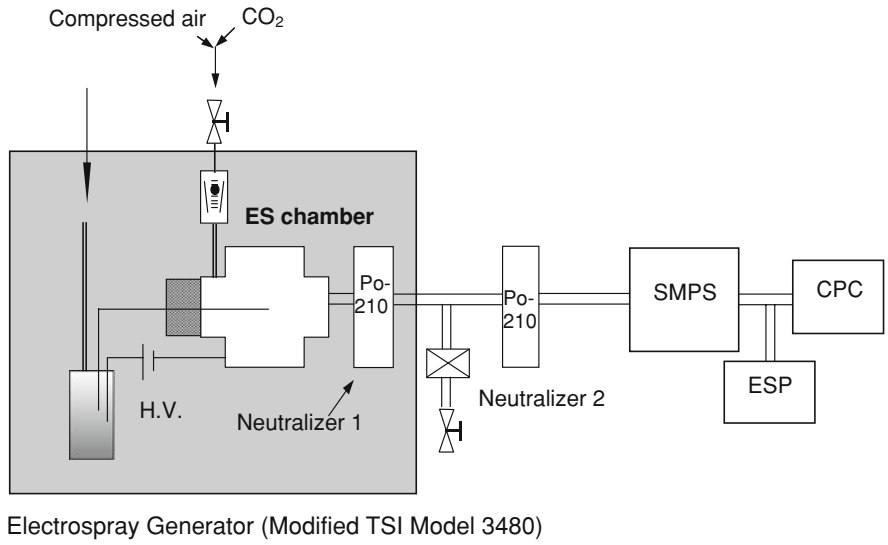

Fig. 1 Experimental setup used to generate SWCNT aerosols using an electrospray system. SMPS: scanning mobility particle sizer; CPC: condensation particle counter; ESP: electrostatic precipitator

(Gorelik et al. 2000). The purified SWCNTs are identical to the material used in the Shvedova et al.'s study (Shvedova et al. 2005). Elemental carbon in SWCNT (HiPCO^{TM}) was assessed according to the NIOSH manual of analytical methods (NMAM) (Birch 2003), whereas metal content (iron) was analyzed by nitric acid dissolution and inductively coupled plasma-atomic emission spectrometry (ICP-AES). Analytical analysis performed by NMAM 5040 and ICP-AES showed that SWCNT comprises 99.7% (wt.) elemental carbon and 0.23% (wt.) iron. For purity assessment of HiPCO^{TM} SWCNT, it was found that >99% of carbon content in the SWCNT HiPCO^{TM} product was accountable in carbon nanotube morphology. The mean diameter and surface area of SWCNT were 1–4 nm and 1,040 m^2g^{-1}. Surface area was determined by Brunauer, Emmett, and Teller (BET) analysis, and the diameter was measured by transmission electron microscopy (TEM). Suspensions were prepared with the purified SWCNTs in buffer solutions (20 millimolar (mM) or 2 mM ammonium acetate in ultrafiltered deionized water), and sonicated for 10–20 min before use. Aqueous suspensions of SWCNTs at three different concentrations (1.0, 2.0, and 5.1 μg mL^{-1}) were tested. The suspension is pushed through a silica capillary tube (25 and 40 μm from TSI and 100 μm ID from Polymicro Technologies) by controlling the pressure difference between its reservoir (1 cm^3 polypropylene vial) and the sharpened end of the tube, held inside an electrospray chamber. The liquid tip is electrified through the solution in the vial, put in electrical contact with a high voltage power supply through a platinum electrode. The droplets generated dried off quickly, and were subsequently neutralized in the electrospray chamber. A sheath air flow of 1.0 L min^{-1} was used and 0.075–0.1 L min^{-1} CO_2 was provided to prevent corona discharge at the capillary tip. The second neutralizer of Po-210 was used to ensure equilibrium charge distribution of the aerosols. The resulting aerosols were analyzed in a scanning mobility particle sizer (SMPS, TSI) using a 3081 long differential mobility analyzer (DMA), and sampled on a TEM grid using an impactor-based electrostatic precipitator (Ku and Maynard 2005) for monodisperse and polydisperse aerosols. For monodisperse aerosols, the mobility size was selected using the DMA. The morphology and agglomeration state of the aerosols were examined by TEM.

Before we investigated the size distributions of SWCNTs generated by electrosprays, it was first necessary to determine the concentration of compact residue particles generated by the complete evaporation of droplets that do not contain any SWCNT particles. These residue particles could interfere with mobility distribution measurements of the SWCNT aerosol in the SMPS. It is desirable that the number of residue particles from the buffer solutions should be as small as possible. Two buffer solutions (20 and 2 mM) were tested. In addition, the effect of capillary sizes on the number concentrations of residue particles was investigated.

Results

Determination of suitable capillary size and buffer solution for electrosprays

We used three capillary sizes (25, 40 and 100 μm ID) to electrospray aqueous SWCNT suspensions. It was difficult to generate SWCNT aerosols with the two capillary sizes (i.e., 25 and 40 μm) due to frequent clogging by SWCNT particles, even with very dilute SWCNT suspensions (1.0 μg mL^{-1}). The SWCNT particles mainly possess large open fibrous morphologies with entangled network of single fibers. Such large structures extend in size to tens of micrometers, and have a tendency to clog the capillary. For the 100 μm capillary, there was no clogging at the concentrations used in this study and this capillary size was sufficient for electrospraying the suspensions.

Figure 2 shows the effect of capillary size and buffer concentrations on the particle size distribution of the residue aerosol resulting from the electrospray of pure buffer solutions. Three combinations of the capillary sizes and buffer concentrations were tested. The number of residue particles generated strongly depends on the buffer concentration. Capillary size seems to have a little effect on the residue particle concentration. As shown in Fig. 2, 40 and 100 μm capillary did not show a significant difference in the number concentration at a given similar liquid flow rate. The figure also shows that 2 mM buffer solution produced a concentration one order of magnitude higher than that produced by 20 mM buffer solution. This is possibly due to the larger initial droplet size generated by the 2 mM buffer solution (the initial

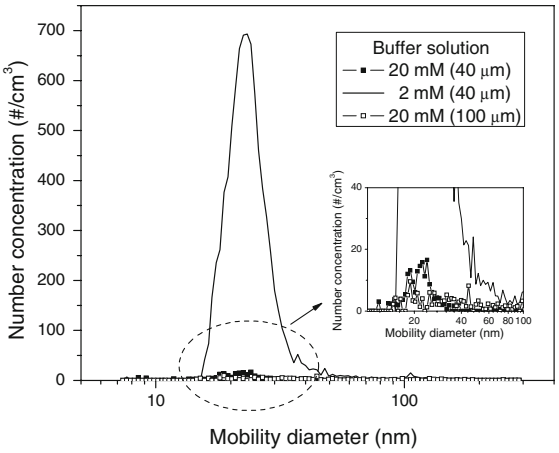

Fig. 2 Size distributions of residue particles generated from buffer solutions for different combinations of capillary sizes and buffer concentrations. The numbers in the parentheses of the legend are capillary sizes used for electrosprays. It is worth noting that 40 and 100 μm capillary using the 20 mM buffer solution did not show a significant difference in the number concentration at a given similar liquid flow rate

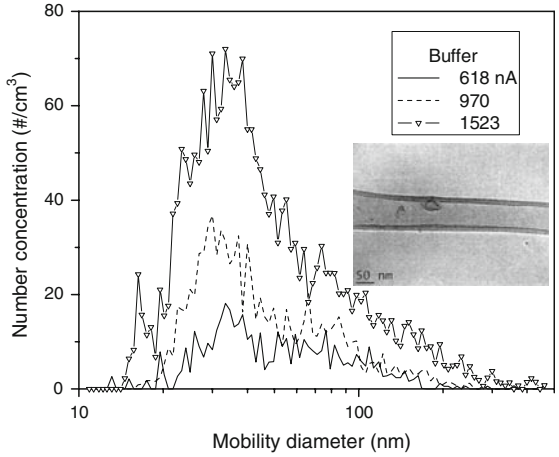

Fig. 3 Size distributions of particles from a buffer solution of 20 mM ammonium acetate in water for various liquid flow rates. The capillary diameter is 100 μm. Spray currents were measured for different flow rates. Liquid flow rates are proportional to spray currents squared according to electrospray theory for highly conducting liquids (Fernandez de la Mora and Loscertales 1994). The figure also shows the typical morphology of the residue particles generated from the buffer solution, which are typically compact and are different from the SWCNT particles

droplet size is inversely proportional to the conductivity of the solution) that subsequently disintegrates to give a large number of smaller residue particles. Based on these observations, all experiments were performed using 20 mM buffer solution and 100 μm capillary sizes to minimize the background residual particle concentration and clogging of the capillary.

The buffer solution was further characterized to estimate the range of particle number concentration with increasing flow rate of the suspension through the capillary. Figure 3 shows the size distributions of residue particles from a 20 mM buffer solution for various liquid flow rates. Spray current was measured at different flow rates, which is proportional to the square root of flow rate (Fernandez de la Mora and Loscertales 1994). The size distributions have a mode between 20 and 30 nm. The total concentration varied from 400 to 1,000 cm^{-3} depending on the flow rate. The figure also shows the typical morphology of the residue particles generated from the buffer solution, which are typically compact and are different from SWCNT particles.

Size distributions of SWCNT aerosols from suspensions with different concentrations

Experiments were conducted to investigate the effect of liquid flow rate through the capillary on the SWCNT

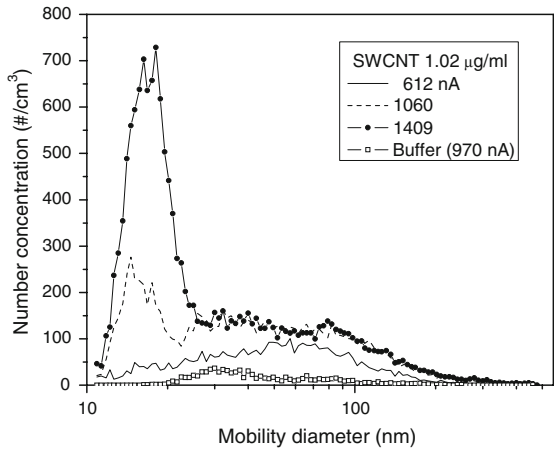

Fig. 4 Size distributions of particles from an SWCNT suspension of 1.02 μg mL^{-1} for various liquid flow rates. Spray currents were measured for different flow rates

aerosol size distribution measured by SMPS. Figure 4 shows the size distributions of particles from an SWCNT suspension of 1.02 μg mL^{-1} for various liquid flow rates, along with that of residue particles from the buffer solution. As spray current increases, the number concentration of SWCNT aerosols also increases. The total number concentration increased

from 4,200 to 15,000 particles cm^{-3}, as spray current increased from 612 to 1,409 nA. These concentrations are one order of magnitude higher than the concentrations of residue particles, indicating low interference from the background residue particles. A new mode appears at around 15–20 nm with increasing flow rate. This mode clearly corresponds to SWCNT aerosols, since the buffer solution without SWCNTs does not have many particles in this size range as shown in Fig. 3. TEM micrographs confirm this observation. Figure 5 shows TEM images of DMA-classified 19 nm mobility diameter particles from the suspension of 1.02 μg mL^{-1}. Most of the particles have fiber-like structures, but do not show individual SWCNT morphologies. The particles look relatively compact, unagglomerated, and fiber-like. Closer observation of the particles in Fig. 5a showed a hollow tube in the center with a diameter around 1.5–2 nm, which corresponds to the diameter of an SWCNT.

Figure 6 shows TEM images of polydisperse particles (particles that were not classified in DMA) from an SWCNT suspension of 1.02 μg mL^{-1}. The SWCNT particles have unique morphology—long nanorope structures that look like straight fibers and seem to be up to several micrometer long.

Size distributions of aerosols from an SWCNT suspension of 2.04 μg mL^{-1} are shown in Fig. 7. The suspension concentration was increased by a factor of two. Compared to the concentration of 1.02 μg mL^{-1}, the size distributions were shifted to the right and a modal diameter appeared at around 35–40 nm. As spray current increased from 930 to 1,483 nA, the total number concentration increased from 13,000 to 27,000 cm^{-3}. Note that the number of residue particles at 1,146 nA is about 1,300 cm^{-3}. At the highest flow rate (spray current 1,483 nA), which corresponds to near maximum flow rate where a spray cone jet is stable, the mode of the size distribution has been changed, indicating that there is a threshold flow rate at which the modal diameter changes. TEM images of the particles with the mobility diameter of 35 nm (that corresponds to the modal diameter of the distribution) are shown in Fig. 8. Closer examination using TEM showed that these particles are relatively compact, short nanotubes, and have physical shape

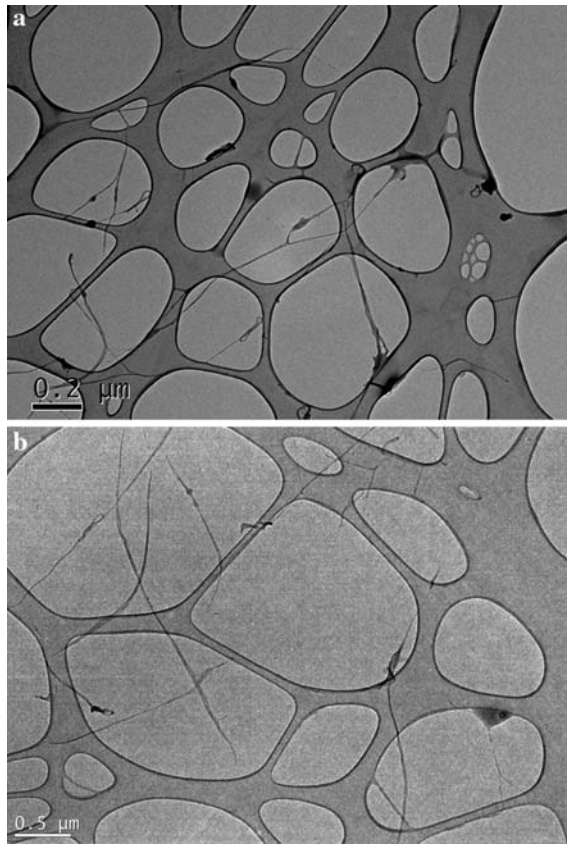

Fig. 6 TEM image of polydisperse particles from a suspension of 1.02 μg SWCNT mL^{-1}

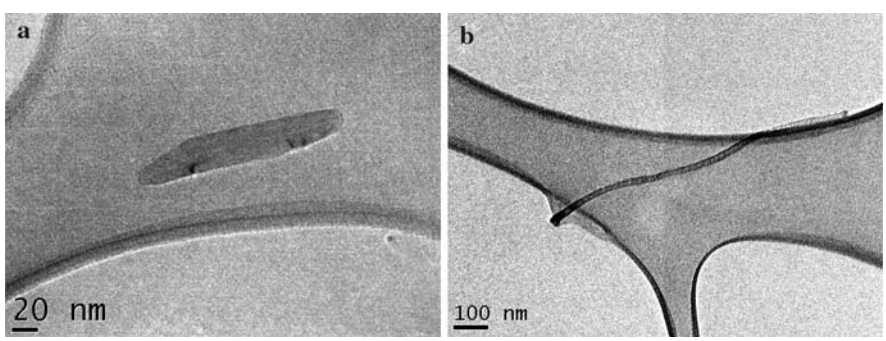

Fig. 5 TEM images of DMA-classified 19 nm mobility diameter particles from an electrosprayed suspension of 1.02 μg SWCNT mL^{-1}

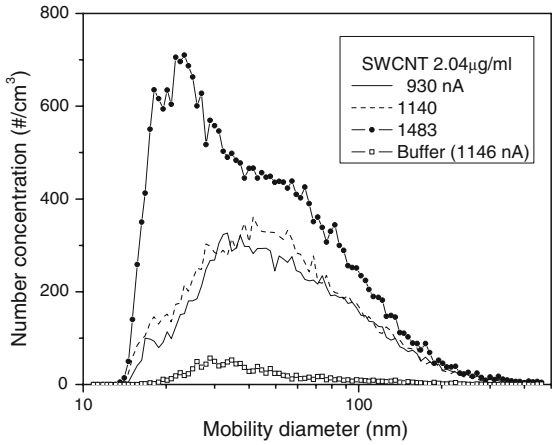

Fig. 7 Size distributions of particles from an SWCNT suspension of 2.04 μg mL^{-1} for various liquid flow rates. Spray currents were measured for different flow rates

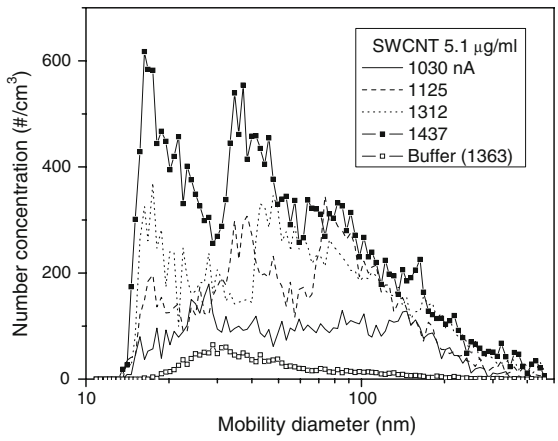

Fig. 10 Size distributions of particles from an SWCNT suspension of 5.10 μg mL^{-1} for various liquid flow rates. Spray currents were measured for different flow rates

similar to 20 nm particles in Fig. 5a. Figure 9 shows typical TEM images of polydisperse particles from the suspension, suggesting that there existed two types of particles: one is long fiber, like the images of the suspension of 1.02 μg mL^{-1} shown in Fig. 6, and the other is low-aspect ratio agglomerate.

Figure 10 shows the size distributions of particles from an SWCNT suspension of 5.10 μg mL^{-1} as a function of liquid flow rates. This suspension concentration is five times higher than the case in Fig. 3. Electrospraying from this high concentration suspension generated a bimodal or trimodal size distribution of aerosols. As spray current increased, the total number concentration increased from 7,300 to 24,900 cm^{-3} and the bimodal size distribution became dominant. At the spray current of 1,437 nA, modal diameters of the size distribution correspond approximately to 20, 40, and 80 nm respectively.

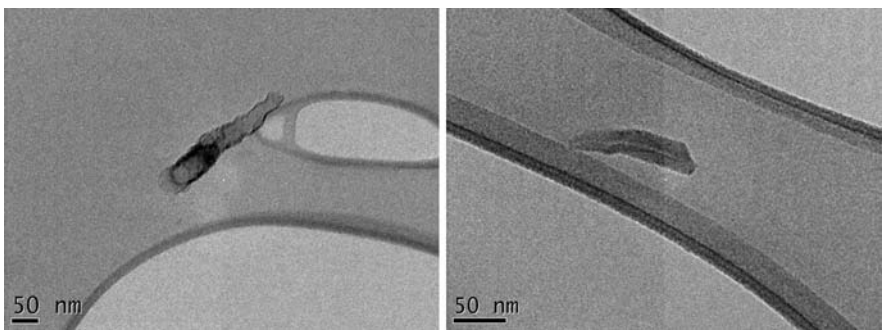

Fig. 8 TEM images of 35 nm monodisperse particles from a suspension of 2.04 μg SWCNT mL^{-1}

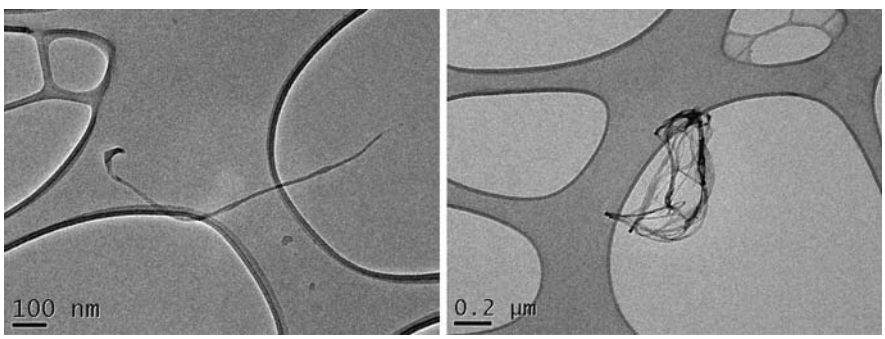

Fig. 9 TEM images of polydisperse particles from a SWCNT suspension of 2.04 μg SWCNT mL^{-1}

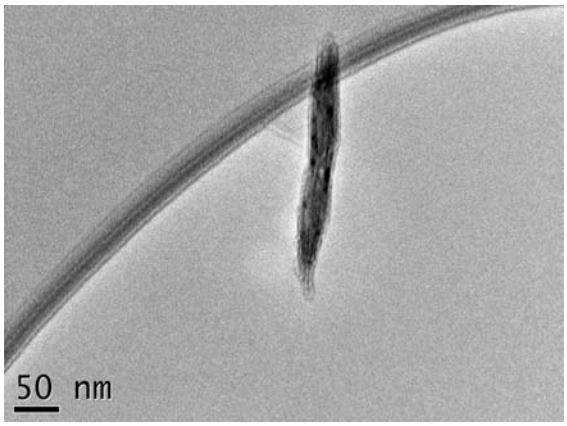

Fig. 11 TEM image of a typical 80 nm monodisperse particle from an SWCNT suspension of 5.10 μg mL^{-1}

Figure 11 shows a TEM image of a typical 80 nm monodisperse particle from the suspension of 5.10 μg mL^{-1}. The particles have fiber-like structures similar to the modal particles in Figs. 5 and 8. Figure 11 shows a particle having aligned structure; closer examination using TEM showed nanotubes that are folded and aligned with a characteristic dimension of each tube of about 2 nm. Figure 12 shows a TEM image of polydisperse particles from the same suspension. It is worth noting that the particles generated have very uniform structures and morphologies. The morphologies of the particles are "ribbon-like" and some of them have long fibers stretched out from the ribbons. The formation of these morphologies may be closely related to electrospray-generated droplet formation and evaporation process. Possible mechanisms for the formation of these particles are discussed below.

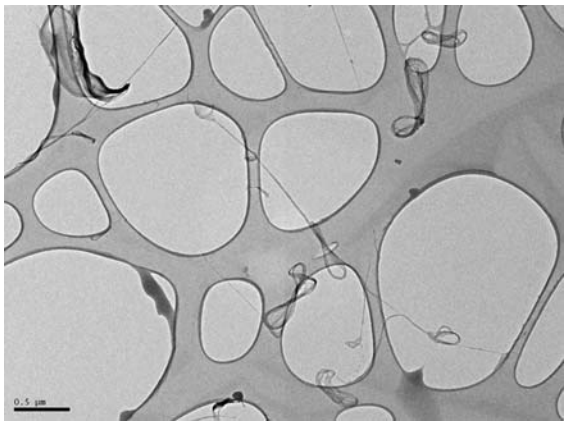

Fig. 12 TEM image of polydisperse particles from a SWCNT suspension of 5.10 μg SWCNT mL^{-1}

Discussion

The effect of SWCNT suspension concentrations on aerosol size distributions

The SWCNT suspension concentrations have been found to affect the size distributions of SWCNT aerosols generated. For lower concentrations of 1.02 and 2.04 μg mL^{-1}, the modal diameters were about 20 and 40 nm, respectively, while several modal diameters such as 20, 40, and 80 nm were observed for higher concentration of 5.1 μg mL^{-1}. The modal diameter can be expected to increase with increasing suspension concentration because more SWCNT particles can exist in a given droplet, which results in solid SWCNT aerosols after complete evaporation of droplets, as shown in Kaufman's work using sucrose (Kaufman 2000). Actually, this results from the Dole's residue model (Dole et al. 1968) where if a non-volatile solute is present in the liquid, the droplet evaporation leaves a residue of this solute. In the Dole's evaporating-droplet model, the residue remains with any specific material present in the droplet (in our study, SWCNTs), which would increase the material's apparent size, and thus shift the mobility diameter. Since electrosprays generate monodisperse droplets, only one peak of the monodisperse aerosols could be expected if, as in the Dole picture, the SWCNTs did not escape from the evaporating droplets, and if every droplet was neutralized so that it could evaporate completely leaving SWCNTs and some residues. However, the appearance of bimodal size distributions at a high suspension concentration of 5.1 μg mL^{-1}, as shown in Fig. 10, is a little bit surprising. This phenomenon may be due to the droplet formation and evaporation in electrosprays. The spray results from the breakup of a jet into charged droplets having initial diameters of several times the fixed diameter of the liquid cone jet. Charged droplet evaporation then gives rise to a series of Coulombic explosions, each leading to the production of many smaller daughter droplets and one mother droplet. The outcome of several generations of such explosions is generally a bidisperse spray of droplets, some relatively large and some relatively small. Complete evaporation of the

large droplets produces bigger particles and evaporation of the small droplets generates smaller particles, as described in a previous article (Ku et al. 2004). These two particles of different sizes may bring bimodal distributions as shown in Fig. 11. On the other hand, Figs. 5 and 7 clearly show that the shift of modal diameter from 20 to 35–40 nm as the concentration increases, which is consistent with the concept of Dole's model. It is worth mentioning that the preliminary study on the generation of an SWCNT aerosol with a much higher concentration than the ones used in this study showed that SWCNT particles with a mode at around 130 nm could be generated, confirming the shift of a modal diameter to a larger size with increasing concentration of SWCNTs.

Particle size-dependent morphology of SWCNTs

We investigated the morphologies of monodisperse and polydisperse SWCNT aerosols. As particle mobility diameter increased in the size range below 100 nm, it was found that they are predominantly single fibers which are 20–50 nm thick and 100–300 nm long. For polydisperse particles, they are long nanoropes with 10–20 nm thick and 1–2 μm long, which look like straight fibers as shown in Fig. 6. These fibers appear to have a well-defined shape and the thickness of the fibers generated is relatively constant, indicating that the electrospray technique can generate SWCNT aerosol particles with controlled morphology. On the other hand, densely agglomerated SWCNT aerosols can be generated from the droplets, as shown in a previous study, using a nebulizer (Shvedova et al. 2005). In our study, ribbon shape particles were observed, as shown in Fig. 12. Shvedova et al. (2005) suggested a possibility in their study that these two morphologies (a dispersed SWCNTs and compact structured SWCNTs, which were much larger than those observed in our study) could bring distinct biological responses in the lungs of mice. It is possible that discrete nanoropes, as shown in Fig. 6, exhibit different toxicity when compared to relatively more compact particles.

Possible mechanisms for the typical particle shape formation

It was observed that two kinds of typical morphologies of SWCNT aerosols can be obtained during the electrospray process. One is ribbon-like and the other is long, straight fiber-like. These two distinct morphologies may be possibly due to the different particle formation mechanisms which would be related to the droplet breakup and evaporation processes. The ribbon-like SWCNT aerosols have relatively compact and low aspect ratios, while the fiber-like aerosols have high aspect ratios. For a given SWCNT suspension of known physical properties such as electrical conductivity and surface tension, the initial droplet sizes to be generated by electrosprays become fixed in a cone-jet mode at a certain liquid flow rate according to the scaling laws of droplet sizes (Fernandez de la Mora and Loscertales 1994; Ganan-Calvo et al. 1997). We did not measure the droplet sizes directly. However, based on the spray currents (I) measured, the initial droplet sizes can be calculated by Eq. 1 as given below (Fernandez de la Mora and Loscertales 1994; Chen and Pui 1997).

$$I = f(\varepsilon)\left(\frac{\gamma K Q}{\varepsilon}\right)^{1/2} \tag{1}$$

where ε is the dielectric constant, γ surface tension, K electrical conductivity, and Q liquid flow rate. The functional form f depends one, and is given by Chen and Pui as follows (Chen and Pui 1997).

$$f(\varepsilon) = -449 - 0.21\varepsilon + 157\varepsilon^{1/6} + 336\varepsilon^{1/6} \tag{2}$$

For the aqueous buffer solution used in this study, $K = 0.2$ Sm^{-1}, $\gamma = 0.072$ Nm^{-1}, and $\varepsilon = 78.4$, and for spray currents shown in Fig. 4, f is calculated as 21.75 and liquid flow rates become 258.6 to 1370.8 nL min^{-1}. These flow rates correspond to initial droplet sizes from 220 to 384 nm. When the suspension is electrosprayed, the spray results from the breakup of a jet into charged droplets having initial diameters of several times the fixed diameter of the capillary jet. When droplets are formed from the jet, SWCNT particles in the suspension move through the jet into the droplets. Some SWCNT particles are smaller than the initial droplet diameter and some are larger. Smaller particles can move easily into the droplets and subsequently get aerosolized. However, for larger agglomerates, larger than the droplet size, the dynamics could be more complicated. It could be hypothesized that a mother droplet leaving the tip of the jet could exert shear forces on a large, coiled SWCNT agglomerate such that it leads to straightening

and/or alignment of individual nanotubes into nanoropes and fibers, leading to well-defined morphologies observed in the experiments. It is worth mentioning that during the experiments, the jet at the tip of the capillary seemed unusually long and elongated when spraying SWCNT particles, possibly due to the presence and accumulation of nanotubes in the liquid jet and the liquid cone as shown in Fig. 13a.

The ribbon-like particle observed in Fig. 12 could be formed by a different mechanism, possibly by the evaporation dynamics of a drying droplet as shown in Fig. 13b. Due to their hydrophobic nature, the nanotubes tend to accumulate at the surface of the droplet. As the droplet undergoes continuous evaporation, an enveloping sheet of nanotubes is formed on the droplet surface, which upon further complete drying gets twisted to form number-eight-like loops as seen Fig. 12. Shvedova et al. (2005) reported relatively compact similar shapes of SWCNT aerosols generated by a nebulizer. It is expected that this type of shape is typical of liquid-based generation methods such as nebulizers and electrosprays. It is also worth noting that for some particles, the number-eight-like loops also appear at the end of long nanoropes in Fig. 12. These particles could be formed by a combination of mechanisms involving the stretching of fiber due to high shear forces and dynamics of droplet evaporation discussed above. Figure 6 shows that the SWCNTs are 1–2 μm in length, which are larger than the initial droplet sizes. The nanotubes in the droplet may conform to the same process as the ribbon shape (or number-eight-like) particle formation. The process for generating the straight, long nanofibers by electrosprays seems to be similar to an electrospinning process in which the liquid jet is being pulled off (Deitzel et al. 2001). The electrospinning occurs when applied to polymer solutions and melts of sufficient viscosities ($\sim$1–200 poise), while electrospraying occurs in the case of low viscosity liquids (Deitzel et al. 2001).

In addition to the above mechanisms, it is also possible that the strong electrical field at the tip of the jet may play a role in determining the fiber morphology. SWCNT particles from electrospray carry high charge, which under the influence of external electrical field may induce its restructuring. Depending on the conductivity of nanotubes and nanoropes, and the mobility of electrical charges within the fibrous network it is possible that these charges may enhance the fiber restructuring

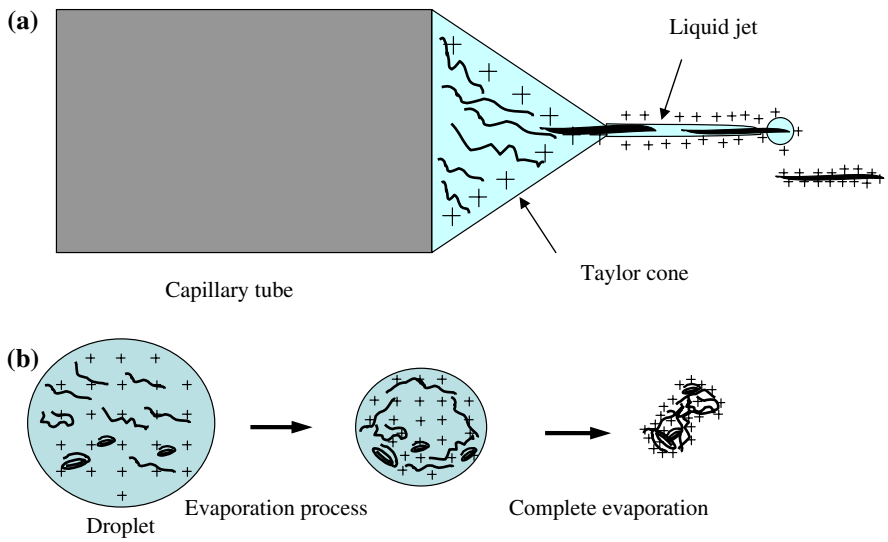

Fig. 13 Schematic diagram showing possible mechanisms for the formation of particle morphologies observed in the experiments. **a** For agglomerates larger than the droplet size, it could be hypothesized that a mother droplet leaving the tip of the jet could exert shear forces on a large, coiled SWCNT agglomerate such that it leads to straightening and/or alignment of individual nanotubes into nanoropes and fibers, leading to well-defined morphologies. **b** Ribbon shape nanotubes may be formed due to the accumulation of hydrophobic nanotubes on the droplet surface and subsequent collapse into twisted sheets due to complete drying of the droplet

to minimize the potential energy of the system. Lilienfeld (1985) reported that clear uncurling of the curled fibers was observed during the application of electric field of the order of several kV cm^{-1} to the fibers. In addition, abrupt unfolding (stretching) of polymer clusters was observed below a critical mass, indicating that polymer (polyethylene glycol) clusters behave as liquid droplets or soft solid particles on reaching the Rayleigh charge limit (Ude et al. 2004). The electric field on the highly conducting droplet surface is expressed as $E = \sigma/\varepsilon_0$, (ε_0 is the permittivity of vacuum and σ is the charge per unit area). According to Gamero-Castaño and Fernandez de la Mora (2000), daughter droplets from the Coulombic explosion are, on the average, at 70 % of the Rayleigh charge limit. If these droplets dry shortly after the explosion, their residue particles could also carry as little as 70 % of the charge limit. Therefore, the electrical field on a 300 nm droplet charged at 70% of the Rayleigh charge limit can be estimated as 3.26×10^3 kV cm^{-1}, which is much higher than the electric field applied in the work by Lilienfeld (1985) for straightening of curved fibers. This extremely high electric field on the particle surface may promote the straightening of curved fibers by Coulombic repulsion.

While any of the above mechanisms are feasible and could explain the observed morphologies, the exact mechanism is not clear. No experiments were designed to further probe each mechanism in the electrospray.

Conclusions

Purified SWCNTs generated by electrospray of aqueous suspensions of SWCNTs were characterized to determine the feasibility of the electrospray method for generating SWCNT aerosols. Experiments were performed to obtain optimum parametric window of electrospray conditions including buffer solution, capillary diameter, flow rate, and suspension concentration to obtain well-defined SWCNT morphologies. Suspension concentration has been found to affect aerosol particle modal size, with particle mobility modal diameter increasing with increasing suspension concentration. In addition, electrospraying from a suspension of higher concentration produced a bimodal distribution of SWCNT aerosols. Monodisperse particles below 100 nm were mostly non-agglomerated, fiber-like particles. The polydisperse particles had two distinct morphologies: ribbon shape and the straight, long fibers. Two possible mechanisms responsible for the observed morphologies were inferred. The first was the formation of twisted sheets (resembling number eight) of nanotubes due to the evaporation dynamics of the droplet, and the second was due to high shear forces generated by droplet breakup and/or high electrical field on particle surface. It was demonstrated that the SWCNT particles with well-defined morphology can be generated using electrosprays.

Acknowledgment This work was funded by the National Institute for Occupational Safety and Health through the National Occupational Research Agenda (NORA) program (Project CAN 9270082).

Disclaimer The mention of any company or product does not constitute an endorsement by the Centers for Disease Control and Prevention. The findings and conclusions in this article are those of the authors and do not necessarily represent the views of the National Institute for Occupational Safety and Health.

References

Baron PA, Sorensen CM, Brockman JE (2001) Nonspherical particle measurements: shape factors, fractals, and fibers. In: Baron PA, Willeke K (eds) Aerosol measurement: principles, techniques, and applications. Wiley, New York, pp 725–726

Birch ME (2003) Elemental carbon monitoring of diesel exhaust particulate in the workplace. In: NIOSH manual of analytical methods (NMAM 5040), Chap Q, 4th edn. NIOSH, Cincinnati, OH (DHHS publication no. 2003-154)

Chen DR, Pui DYH (1997) Experimental investigation of scaling laws for electrospraying: dielectric constant effect. Aerosol Sci Technol 27:367–380

Deitzel JM, Kleinmeyer J, Harris D, Tan NCB (2001) The effect of processing variables on the morphology of electrospun nanofibers and textiles. Polymer 42(1):261–272

Dole M, Mach LL, Hines RL, Mobley RC, Ferguson LP, Alice MB (1968) Molecular beams of macroions. J Chem Phys 49:2240–2249

Fernandez de la Mora J, Loscertales IG (1994) The current emitted by highly conducting Taylor cones. J Fluid Mech 260:155–184

Gamero-Castaño M, Fernandez de la Mora J (2000) Mechanisms of electrospray ionization of singly and multiply charged salt clusters. Anal Chim Acta 406:67–91

Ganan-Calvo AM, Davila J, Barrero A (1997) Current and droplet size in the electrospraying of liquids. Scaling laws. J Aerosol Sci 28:249–275

Gorelik O, Nikolaev P, Arepalli S (2000) Purification procedures for single-walled carbon nanotubes, NASA

contractor report. NASA, Hanover, MD (NASA/CR-2000-208926)

Kaufman SL (2000) Electrospray diagnostics performed by using sucrose and proteins in the gas-phase electrophoretic mobility molecular analyzer (GEMMA). Anal Chim Acta 406:3–10

Kim SC, Pui DYH (2005) Delivery of single nanoparticles (NP) to cells using an electrospray system [abstract]. In: 2nd international symposium on nanotechnology, occupational health, Minneapolis, Minnesota, 3–6 October 2005, p 80

Ku BK (2007) Characterization of purified single walled carbon nanotube aerosols generated by electrospraying of suspensions. In: 3rd international symposium on nanotechnology, occupational and environmental health, Taipei, Taiwan, Aug 29–Sep 1 2007, pp 11–12

Ku BK, Maynard AD (2005) Comparing aerosol surface-area measurement of monodisperse ultrafine silver agglomerates using mobility analysis, transmission electron microscopy and diffusion charging. J Aerosol Sci 36: 1108–1124

Ku BK, Maynard AD (2006) Generation and investigation of airborne silver nanoparticles with specific size and morphology by homogeneous nucleation, coagulation and sintering. J Aerosol Sci 37:452–470

Ku BK, Fernandez de la Mora J, Saucy DA, Alexander JNIV (2004) Mass distribution measurement of water-insoluble polymers by charge-reduced electrospray mobility analysis. Anal Chem 76(3):814–822

Ku BK, Maynard AD, Baron PA, Deye GJ (2007) Observation and measurement of anomalous responses in a differential mobility analyzer caused by ultrafine fibrous carbon aerosols. J Electrostat 65:542–548

Lam CW, James JT, McCluskey R, Hunter RL (2004) Pulmonary toxicity of single-wall carbon nanotubes in mice 7 and 90 days after intratracheal instillation. Toxicol Sci 77:126–134

Lam CW, James JT, McCluskey R, Arepalli S, Hunter RL (2006) A review of carbon nanotube toxicity and assessment of potential occupational and environmental health risks. Crit Rev Toxicol 36:189–217

Lilienfeld P (1985) Rotational electrodynamics of airborne fibers. J Aerosol Sci 16(4):315–322

Maynard AD, Baron PA, Foley M, Shvedova AA, Kisin ER, Castranova V (2004) Exposure to carbon nanotube material: aerosol release during the handling of unrefined single walled carbon nanotube material. J Toxicol Environ Health 67(1):87–107

Maynard AD, Ku BK, Emery MS, Stolzenburg MR, McMurry PH (2007) Measuring particle size-dependent physicochemical structure in airborne single walled carbon nanotube agglomerates. J Nanopart Res 9:85–92

Nakaso K, Fujimoto T, Seto T, Shimada M, Okuyama K, Lunden MM (2001) Size distribution change of Titania nano-particle agglomerates generated by gas phase reaction, agglomeration, and sintering. Aerosol Sci Technol 35:929–947

Nakaso K, Shimada M, Okuyama K, Deppert K (2002) Evaluation of the change in the morphology of gold nanoparticles during sintering. J Aerosol Sci 33:1061–1074

Oberdörster G, Maynard A, Donaldson K, Castranova V, Fitzpatrick J, Ausman K, Carter J, Karn B, Kreyling W, Lai D, Olin S, Monteiro-Riviere N, Warheit D, Yang H (2005) Principles for characterizing the potential human health effects from exposure to nanomaterials: elements of a screening strategy. Part Fibre Toxicol 2:1–110. doi: 10.1186/1743-8977-2-8

Poland CA, Duffin R, Kinloch I, Maynard A, Wallace WAH, Seaton A, Stone V, Brown S, MacNee W, Donaldson K (2008) Carbon nanotubes introduced into the abdominal cavity of mice show asbestos-like pathogenicity in a pilot study. Nat Nanotechnol (Published online: 20 May 2008). doi:10.1038/nnano.2008.111

Scott CD, Povitsky A, Dateo C, Gokcen T, Willis PA, Smalley RE (2003) Iron catalyst chemistry in modeling a high-pressure carbon monoxide nanotube reactor. J Nanosci Nanotechnol 3:63–73

Shvedova AA, Kisin ER, Murray AR, Gandelsman VZ, Maynard AD, Baron PA, Castranova V (2003) Exposure to carbon nanotube material: assessment of the biological effects of nanotube materials using human keratinocyte cells. J Toxicol Environ Health 66(20):1909–1926

Shvedova AA, Kisin ER, Mercer R, Murray AR, Johnson VJ, Potapovich AI, Tyurina YY, Gorelik O, Arepalli S, Schwegler-Berry D, Hubbs AF, Antonini J, Evans DE, Ku BK, Ramsey D, Maynard A, Kagan VE, Castranova V, Baron P (2005) Unusual inflammatory and fibrogenic pulmonary responses to single-walled carbon nanotubes in mice. Am J Physiol Lung Cell Mol Physiol 289:L698–L708

Stern ST, McNeil SE (2008) Nanotechnology safety concerns revisited. Toxicol Sci 101(1):4–21

Ude S, Fernandez de la Mora J, Thomson BA (2004) Charge-induced unfolding of multiply charged polyethylene glycol ions. J Am Chem Soc 126:12184–12190

Warheit DB (2006) What is currently known about the health risks related to carbon nanotube exposures? Carbon 44: 1064–1069

Warheit DB, Laurence BR, Reed KL, Roach DH, Reynolds GAM, Webb TR (2004) Comparative pulmonary toxicity assessment of single-wall carbon nanotubes in rats. Toxicol Sci 77:117–125